REPORT DOCUMENTATION PAGE

Form Approved
OMB NO. 0704-0188

1. AGENCY USE ONLY (Leave Blank)	2. REPORT DATE	3. REPORT TYPE AND DATES COVERED
	August 11, 2004	Final 6/1/2001 – 28/2/05

4. TITLE AND SUBTITLE
Long-Distance, High Data-Rate Quantum Communication with Ultralow Loss Photonic Band Gap Fiber

5. FUNDING NUMBERS
DAAD19-01-1-0647

6. AUTHOR(S)
Prof. Yoel Fink

7. PERFORMING ORGANIZATION NAME(S) AND ADDRESS(ES)
Massachusetts Institute of Technology
Research Laboratory of Electronics
77 Massachusetts Avenue
Cambridge, MA 02139

8. PERFORMING ORGANIZATION REPORT NUMBER

9. SPONSORING / MONITORING AGENCY NAME(S) AND ADDRESS(ES)
U. S. Army Research Office
P.O. Box 12211
Research Triangle Park, NC 27709-2211

10. SPONSORING / MONITORING AGENCY REPORT NUMBER
42671.1-PH-QC

11. SUPPLEMENTARY NOTES
The views, opinions and/or findings contained in this report are those of the author(s) and should not be construed as an official Department of the Army position, policy or decision, unless so designated by other documentation.

12 a. DISTRIBUTION / AVAILABILITY STATEMENT
Approved for public release; distribution unlimited.

12 b. DISTRIBUTION CODE

13. ABSTRACT (Maximum 200 words)

We are pleased to report substantial progress across the entire cylindrical photonic bandgap fiber project. This project's main objective is the development of ultra low-loss hollow photonic bandgap fibers for quantum communications applications. Specifically, the following objectives have been met: the worlds first automated preform fabrication system for low loss photonic bandgap fibers was specified, designed, ordered, manufactured and installed. This system will enable the fabrication of fibers with low defect counts critical to the achievement of the program's objectives. A new material compatible with our fabrication process was identified leading to a substantial decrease in lattice period. Photonic bandgap fibers that exhibit the smallest lattice period ever reported, with individual layers that are 60nm in thickness have been drawn. Extended lengths of fibers with primary photonic bandgaps at 850nm and 1600nm were fabricated, the characterization and improvement of their properties is a major objective for the next year. Quantum interference was demonstrated through a short length of PBG fibers, a necessary condition for entangled photon transmission. A novel coupling technique using a spatial phase modulator has been developed this represents a critical step towards the realization of low loss fibers based on low loss TE01 mode transmission. Finally we have created the world's first M-I-S fibers for dual electron photon transport and device applications.

14. SUBJECT TERMS			15. NUMBER OF PAGES
			16. PRICE CODE
17. SECURITY CLASSIFICATION OR REPORT	18. SECURITY CLASSIFICATION ON THIS PAGE	19. SECURITY CLASSIFICATION OF ABSTRACT	20. LIMITATION OF ABSTRACT
UNCLASSIFIED	**UNCLASSIFIED**	**UNCLASSIFIED**	**UL**

Report for QuIST Project
Yoel Fink
July 2004

Abstract:

We are pleased to report substantial progress across the entire cylindrical photonic bandgap fiber project. This project's main objective is the development of ultra low-loss hollow photonic bandgap fibers for quantum communications applications. Specifically, the following objectives have been met: the worlds first automated preform fabrication system for low loss photonic bandgap fibers was specified, designed, ordered, manufactured and installed. This system has enabled the fabrication of fibers with low defect counts and very large number of periods critical to the achievement of the program's objectives. New materials compatible with our fabrication process were discovered leading to a substantial decrease in lattice period. Materials selection criteria were identified and analytical models for ultimate feature size were developed. Photonic bandgap fibers that exhibit the smallest lattice period ever reported, with individual layers that are below 50nm in thickness. Extended lengths of fibers with primary photonic bandgaps at 400nm and above were fabricated, the characterization and improvement of their properties is a major objective for the next year. Quantum interference was demonstrated through a short length of PBG fibers, a necessary condition for entangled photon transmission. A novel coupling technique using a spatial phase modulator has been developed this represents a critical step towards the realization of low loss fibers based on low loss TE_{01} mode transmission. Finally we have created the world's first M-I-S fibers for dual electron photon transport and device applications

Report:

Over the past year substantial progress has been made across the entire cylindrical photonic bandgap quantum transmission fiber project, specifically the following milestones have been accomplished:

1. An automated preform fabrication system for low loss photonic bandgap fibers, specified, designed, ordered, installed.
2. Analytical materials selection criteria developed.
3. Structural and optical characterization of photonic bandgap fibers for high frequency transmission performed.
4. Quantum interference demonstrated through high frequency PBG fibers.

5. New coupling technique for PBG fibers using spatial phase modulators was developed.
6. New fibers developed that are relevant to both low loss transmission and entangled photon generation.
7. New metal-semiconductor-insulator fibers developed.

We have recently received and installed the world's first fully automated preform fabrication system for photonic bandgap fibers. This system will enable unprecedented control over layer dimensions and is expected to substantially decrease the density of defects and enhance the fiber material purity. This novel system is based on a roll-to-roll technique, utilizing thermal evaporation in four independently controlled deposition stations to coat a polymer web on both sides with the required film thickness. The system was developed, designed and specified at MIT and manufactured at System Design Inc. A schematic and photos of the installed system are presented in Appendix A. The automated preform fabrication system is expected to significantly contribute to the improvement of shorter wavelength fibers commensurate with the entangled source produced by Dr. Wong.

We have improved our understanding of the conditions on the materials properties which enable their codrawing to low loss fiber. We have introduced a new polymer material – poly-ether imide (PEI) with improved properties into our process, this enabled the fabrication of short wavelength cylindrical PBG fibers. We have introduced a new high index glass As2S3. This was afforded by a high temperature surface energy measurement system that we purchased and have used in the study of interfacial energy contributions in our multiple interface fiber. A description of the system and some of the initial results are described in Appendix B.

Fibers at short wavelengths have been produced and the characterization effort is currently a major focus of our efforts. We are about to submit an important publication on our findings which is enclosed in Appendix C.

We have made preliminary characterization of the PBG fiber for propagation of entangled photon pairs at 797 nm. We used a high-flux source of orthogonally polarized photon pairs that has previously been characterized with a quantum interference visibility of 99% (quant-

ph/0305092). We coupled these photon pairs through a 10-cm-long PBG fiber that was optimized for ~800-nm transmission. At the output we measured a quantum interference visibility of 96.3%, which suggests that quantum correlation, and hence entanglement, can be effectively transmitted through the PBG fiber with little degradation. We have observed, however, significant transmission loss due to coupling and PBG fiber attenuation. Interestingly, it seems that the survival rate of the photon pairs (by coincidence counting and quantum interference measurement) is higher than that expected from the observed attenuation of the singles. We are continuing our investigation of the entanglement transmission properties of the PBG fiber. Additional details of the results are presented in Appendix D.

Our theoretical predictions have identified the TE01 as the lowest loss mode. This mode has a peculiar electric field pattern which is pointed in the circumferential direction and thus has a very small overlap with a typical laser mode. To that end we have developed a coupling technique which utilizes a spatial phase and amplitude modulator to shape the incoming wavefront as to maximize the coupling to the low loss mode. The details of the coupling scheme are presented in Appendix E.

Our leadership position in the development of PBG fibers has manifested itself in the development of two novel fiber structures this year. These are a direct result of our deeper understanding of the materials selection and fabrication techniques. We recently demonstrate the fabrication of a fiber made of conducting, semiconducting and insulating elements. A preform based fiber drawing technique is used to achieve feature sizes which are below 100nm in a variety of geometries. To demonstrate the utility of our approach two new types of functional fibers are introduced: hybrid photonic bandgap fibers capable of conducting both photons and electrons, and metal-semiconductor-metal fibers designed for distributed light detection. The hybrid photonic bandgap fibers guide light through a hollow core surrounded by a multilayer omnidirectional dielectric mirror while conducting electrons through an array of metal filaments. The distributed light detecting fibers consist of a solid cylindrical glassy semiconductor core in contact with two metal electrodes, and which the optical and electrical properties drastically change when illuminated. The materials combination, fabrication approach, and device structures

demonstrated here may enable a broad range of novel electronic and photonic applications in fiber form. A manuscript describing these novel fibers is presented in appendix F.

Appendix A

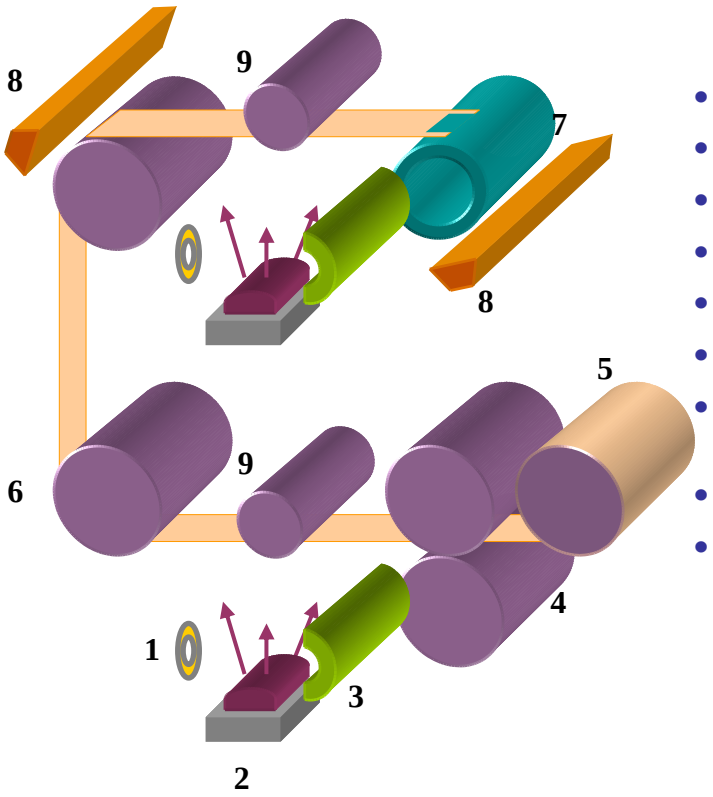

- Thickness monitor
- Evaporation source
- Shutter
- Motorized capstan
- Polymer film feed roll
- Idler roll
- Take-up/preform substrate
- Heater
- Chilling roll or removable roll for outside deposition on top of a rod

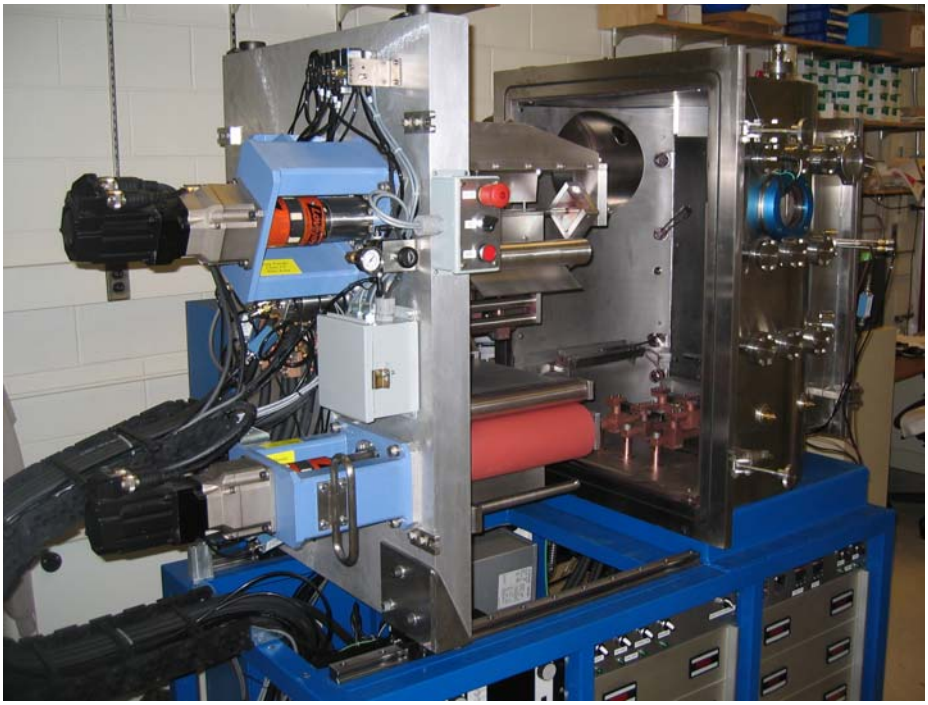

Appendix B

Material	Temp. (°C)	Contact angle	**Calculated interfacial Energy (mJ/m^2)**
As_2Se_3 on PES film	~292	126.6 +/- 2.5	**114 +/- 9**

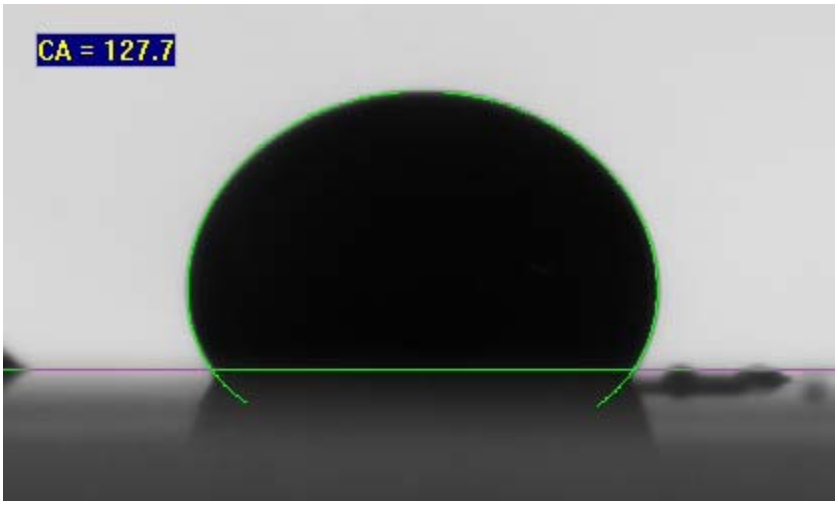

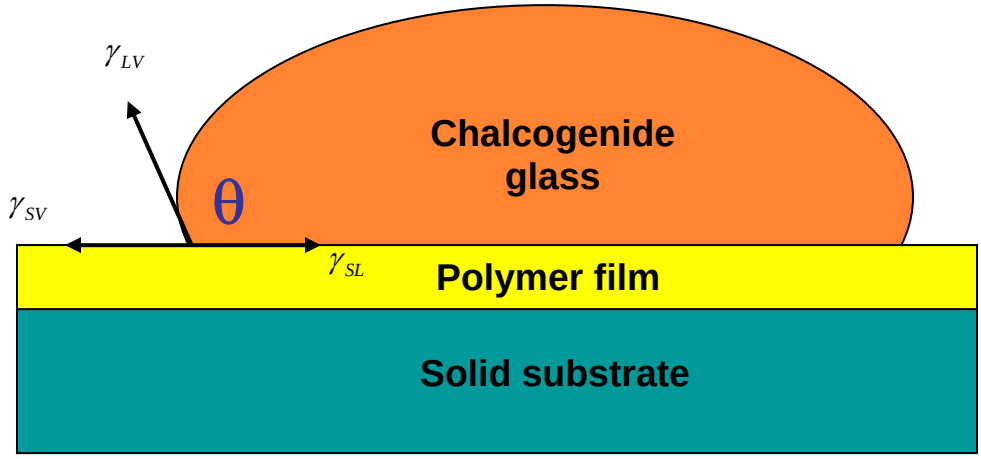

Appendix C

High Frequency Cylindrical Photonic Bandgap Fibers for 0.85 to 1.55 μm Transmission

Research laboratory of Electronics and
Department of Materials Science and Engineering
Massachusetts Institute of Technology
Cambridge, Massachusetts 02139, USA

Abstract

Hollow-core photonic bandgap fibers can be divided into two distinct classes: those made from a 2-D lattice of air holes in silica and those made from a cylindrical multilayer composite structure. Here we report for the first time the fabrication of hollow-core cylindrical photonic bandgap fibers with fundamental photonic bandgaps at near-infrared wavelengths, from 0.85 to 1.55 μm. The fibers are drawn from a multilayer preform into extended lengths of fiber. Light is guided in the fibers through a large hollow-core that is lined with an interior omnidirectional dielectric mirror that creates large photonic bandgaps. We extend the range of materials that can be used in these fibers to include poly(ether imide) (PEI) in addition to the arsenic triselenide (As_2Se_3) glass and poly(ether sulfone) (PES) that have been used previously. Further, we have characterized the refractive indices of these materials over a broad wavelength range (0.4 – 15 μm) and incorporated the measured optical properties into calculations of the fiber photonic band structure.

Introduction

Intensive research by academic, industrial, and governmental laboratories around the world has been done on devices using photonic bandgap materials (1-3). Some of the most successful demonstrations to date have involved photonic bandgap guidance in optical fibers, including light propagation through hollow-core fibers.

Hollow-core photonic bandgap fibers can be divided into two distinct classes: those made from a 2-D photonic crystal lattice of air holes in a solid dielectric (4-6) and those made from a cylindrical multilayer composite structure (also called 1-D photonic crystal fibers or Bragg fibers) (7). Recently, researchers have reported on hollow-core photonic bandgap fibers with low losses around 1.5 μm (8) and 850 nm (9) based on silica-air 2-D photonic crystal structures. In addition, researchers have made use of the tailorable dispersion and nonlinear characteristics of these fibers to demonstrate novel effects in ultrafast pulse propagation and the nonlinear optics of gases (10,11).

Here we report new work on the second major type of photonic bandgap fiber; cylindrical photonic bandgap fibers (also called 'Bragg fibers') that have the ability to confine light in a low-index or hollow-core (7). These fibers consist of multiple alternating layers of high- and low-index materials surrounding a cylindrical hollow core. Hollow-core guiding versions of these fibers have only recently been successfully fabricated, with fundamental photonic bandgaps at 3 and 10.6 μm wavelength (12). While those wavelengths may be used for high-energy laser delivery, it is also of interest to explore the usage of these fibers at near-infrared (IR) wavelengths where most modern solid-state lasers operate, enabling applications ranging from standard telecommunications to ultrafast physics. In particular, those fibers that have a large refractive index contrast between the layer materials have been shown theoretically to allow great reductions in fiber absorption and non-linearities as well as widely tunable dispersion and other interesting properties (13-17). The high refractive index contrast between the layer materials leads to large photonic bandgaps and makes the inner lining of the fiber analogous to an omnidirectional dielectric mirror (18,19). This structure should therefore have short electromagnetic penetration depths within the layer structure, minimizing the interaction of light with the layer materials (20). Here we report for the first time the fabrication of hollow-core guiding cylindrical photonic bandgap fibers at near-IR wavelengths, from 0.85 to 1.55 μm, requiring a significant reduction in feature size from previous work.

Another important goal in the further development of these fibers is an expansion of the suite of materials that can be successfully employed in their production. The chosen materials must have compatible viscous and thermodynamic properties in order to be fabricated into a multilayer preform and drawn at high temperature into a fiber. To broaden the scope of these efforts, we have chosen to incorporate poly(ether imide) (PEI) into the mirror layer structure of these fibers, in addition to the arsenic triselenide (As_2Se_3) and poly(ether sulfone) (PES) that have been used in the past. It is also important to gain a deeper understanding of the properties of these materials and how they influence the photonic bandgap behavior in these fibers. To this end, we have performed broadband (0.4-15 μm) spectroscopic ellipsometry measurements on PEI, PES, and As_2Se_3 and incorporated the resulting experimentally determined real and imaginary refractive index values into photonic band diagram calculations for PEI and As_2Se_3.

Experimental

Refractive indices of As_2Se_3, PEI and PES were measured using a SOPRA broadband spectroscopic ellipsometer. As_2Se_3 films were prepared by thermal evaporation onto a silicon substrate. PEI and PES were prepared by spin coating from polymer solutions onto silicon substrates. The nominally stoichiometric composition of the evaporated As_2Se_3 films was verified by electron microprobe analysis. The As_2Se_3 films were confirmed to be amorphous both before and after fiber drawing by Raman microprobe spectroscopy.

The fiber preform was fabricated by the thermal evaporation of an As_2Se_3 layer (2-5 μm) on each side of a free-standing 9-15-μm-thick PEI film, and the subsequent 'rolling' of that coated film into a hollow multilayer tube. This hollow macroscopic pre-form was consolidated by heating under vacuum, and clad with a thick outer layer of PES; the layered preform was then placed in an optical fiber draw tower, and drawn down into hundreds of meters of fiber having well controlled submicrometer layer thicknesses and photonic bandgaps in the near-IR. The spectral positions of the photonic bandgaps were controlled by the optical monitoring of the

outer diameter of the fibers during draw. Typical standard deviations in the fiber outer diameter were ~1-2% of that diameter.

Fiber transmission spectra in the near to mid-IR were measured with a Fourier-transform infrared (FTIR) spectrometer (Bruker Optics Tensor 37), using a lens to couple light into the fiber and an external detector. At shorter wavelengths, white light from a quartz tungsten halogen (QTH) lamp was coupled into the fibers and measured using a StellarNet EPP2000 spectrometer.

Results and Discussion

Scanning electron microscope (SEM) imaging (Fig.1) of a hollow-core cylindrical bandgap fiber with a fundamental bandgap of 0.85 μm reveals that the drawn fiber maintains proportional layer thickness ratios, and that the PEI and As_2Se_3 films adhere well during rigorous thermal cycling and elongation. Within the multilayer structure shown in Fig.1 (C), the PEI layers (grey) have a thickness of 200 nm, and the As_2Se_3 layers (bright) are 60 nm thick (except for the first and last As_2Se_3 layers, which are 30 nm).

The real component of the refractive indices of PEI, PES, and As_2Se_3 are compared in Fig. 2. At 1.55 μm, the refractive indices of PEI, PES, and As_2Se_3 are 1.66, 1.62, and 2.82, respectively. The Fig. 2 inset shows the refractive indices of those materials up to 15 μm. The polymeric materials have significant vibrational absorption bands from 5 μm to 15 μm, resulting in sharp index variations. The As_2Se_3 has a large, smooth change in refractive index (as well as an increase in absorption) from 400 to 800 nm due to its material electronic bandgap around 3 eV. These results of the real and imaginary (not shown) index measurements were both used for the calculation of the photonic band diagram shown in Fig. 3. This was important in order to obtain the proper agreement between the band diagram and experiment, particularly for those fibers having high-order bandgaps at wavelengths near or beyond the As_2Se_3 electronic bandgap.

Fig. 3 shows the photonic band diagram for an As_2Se_3 / PEI multilayer mirror calculated using Bloch wave / eigenvalue techniques (assuming an infinite periodic multilayer structure) (3). This diagram was calculated using the experimental parameters (layer thicknesses and indices) of a fiber fabricated with a fundamental bandgap at the telecommunications wavelength of ~1.55 μm. The PEI and As_2Se_3 layers were determined to be 300 and 150 nm, respectively, with SEM analysis.

These parameters were used to calibrate the right-hand wavelength axis of the band diagram. The measured transmission spectrum for this same fiber is shown in Fig. 4. Good agreement is found between the relative positions and bandwidths of the first three measured and calculated bandgaps, verifying that transmission through the fiber is dominated by the photonic bandgap mechanism. The visible green color of the output from the fiber end (Fig. 3 inset) corresponds to the third-order bandgap around 550 nm. These colors from high-order photonic bandgaps are also visible externally through the cladding of the fibers (Fig.5).

Fig.6 shows an output field pattern of a fiber-coupled QTH lamp from a hollow-core photonic bandgap fiber held nominally straight. The fiber was 30 cm long, and the fiber hollow core is 241 μm in diameter. The wavelengths detected in this image ranged from ~0.4 to 1.8 μm. Although the output appears Gaussian, due to the large core size and observations of multimode propagation through the core, we expect that this output field pattern is comprised of a superposition of many modes at different wavelengths.

As mentioned previously, the spectral positions of the photonic bandgaps were controlled by the laser monitoring of the outer diameter of the fibers during draw. Fibers with an

outer diameter of 1.218 and 509 μm have fundamental bandgaps at 1.47 and 0.85 μm, respectively. Fig. 7 shows the wavelength scalability of these fibers, with the comparison of the transmission spectra for six different fibers. These six fibers have fundamental bandgaps centered at 1.47, 1.39, 1.27, 1.03, 0.93 and 0.85 μm, respectively. These wavelengths span a range covering the laser lines of many commercially important lasers, such as Nd:YAG at 1.06 μm, and laser diodes at 0.85 μm.

Initial estimates for the transmission losses of these fibers have shown that the losses remain high compared to other reported hollow-core photonic bandgap fibers at these wavelengths (8,9). We are working to complete these loss measurements and describe them in terms of the appropriate loss mechanisms. Potential sources of loss include: 1) the highly multimode nature of these fibers, facilitating coupling to lossy high-order modes; 2) fabrication defects such as dust or the formation of crystallites in As_2Se_3; and 3) non-uniformity in the layer structure introduced from roughness of the initial films, preform fabrication, or fiber drawing. It should be feasible to systematically reduce each one of these loss mechanisms and ultimately to demonstrate fiber transmission losses that are much lower than the intrinsic layer material losses, as has already been demonstrated at 10.6 μm in our previous work. Further analysis is needed to quantify the relative importance of each one of these proposed loss mechanisms.

Conclusion

In summary, cylindrical photonic bandgap fibers have been fabricated for the first time with fundamental photonic bandgaps at wavelengths ranging from 0.85 to 1.55 μm. These fibers rely on an interior omnidirectional dielectric mirror lining to guide light through a hollow core. We have incorporated a new material into the fiber layer structure, PEI, and compared its optical properties to the previously used As_2Se_3 and PES. This work demonstrates the wavelength and small-feature size scalability of the materials and processes employed, as well as the potential for the application of these fibers at standard telecommunications and solid-state laser wavelengths.

References

1. Yablonovitch, E. Inhibited Spontaneous Emission in Solid-State Physics and Electronics. Physical Review Letters 58, 2059-2062 (1987).
2.J ohn, S. Strong Localization of Photons in Certain Disordered Dielectric Superlattices. Physical Review Letters 58, 2486-2489 (1987).
3. Joannopoulos, J. D., Meade, R. D. & Winn, J. N. Photonic Crystals: molding the flow of light. (Princeton University Press, Princeton, New Jersey, 1995).
4. Cregan, R. F. et al. Single-Mode Photonic Band Gap Guidance of Light in Air. Science 285, 1537-1539 (1999).
5. Allan, D. C. et al. in Photonic Crystals and Light Localization in the 21st Century (ed. Soukoulis, C. M.) (Kluwer, 2001).
6. Eggleton, B. J., Kerbage, C., Westbrook, P. S., Windeler, R. S. & Hale, A. Microstructured optical fiber devices. Optics Express 9, 698-713 (2001).
7. Yeh, P., Yariv, A. & Marom, E. Theory of Bragg Fiber. Journal of the Optical Society of America 68, 1196-1201 (1978).
8.C. M. Smith, N. Venkataraman, M. T. Gallagher, D. Muller, J. A. West, N.F. Borrelli, D. C. Allan and K. W. Koch, Nature 424, 657-659 (2003).
9. G. Bouwamans, F. Laun, J.C. Knight, P.St. J.Russell, L. Farr, B.J.Mangan, and H.Sabert Properties of a hollow-core photonic bandgap fiber at 850 nm wavelength. Optics Express 11, 1613-1620 (2003).
10.D. G. Ouzounov, F. R. Ahmad, D. Muller, N. Venkataraman, M. T. Gallagher, M. G. Thomas, J. Silcox, K. W. Koch, and A. L. Gaeta Generation of megawatt optical solitons in hollow-core photonic band-gap fibers, Science 301, 1702-1704 (2003).
11. F. Benadid, J. C. Knight, G. Antonopoulos, P. St. J. Russell Stimulated raman scattering in hydrogen-filled hollow-core photonic crystal fiber. Science 298, 399-402 (2002).
12. B. Temelkuran, S. D. Hart, G. Benoit, J D. Joannopoulos and Y. Fink Nature 420, 650-653 (2002).
13. Ibanescu, M., Fink, Y., Fan, S., Thomas, E. L. & Joannopoulos, J. D. An all-dielectric coaxial waveguide. Science 289, 415-419 (2000).
14. Johnson, S. G. et al. Low-loss asymptotically single-mode propagation in large-core OmniGuide fibers. Optics Express 9, 748-779 (2001).
15. Fink, Y. et al. Guiding optical light in air using an all-dielectric structure. Journal of Lightwave Technology 17, 2039-2041 (1999).
16.M. Soljacic, M. Ibanescu, S. G. Johnson, J.D.Joannopoulos, and Yoel Fink Optical Bistability in Axially Modulated OmniGuide Fibers, Optics Letters 28, 516 (2003).
17. T. D. Engeness, M. Ibanescu, S. G. Johnson, O. Weisberg, M. Skorobogatiy, S. Jacobs, and Y. Fink Dispersion tailoring and compensation by modal interactions in OmniGuide fibers Opt. Express 11, 1175-1198 (2003).
18. Fink, Y. et al. A dielectric omnidirectional reflector. Science 282, 1679-1682 (1998).
19. Hart, S. D. et al. External Reflection from Omnidirectional Dielectric Mirror Fibers. Science 296, 510-513 (2002).
20. M. Ibanescu, S. G. Johnson, M. Soljacic, J. D. Jonnopoulos, Y. Fink, O. Weisberg, T. D. Engeness, S. A. Jacobs, and M. Skorobogatiy, Analysis of mode structure in hollow dielectric waveguide fibers, Phys. Rev. E, 67, 046608-1-8, (2003).

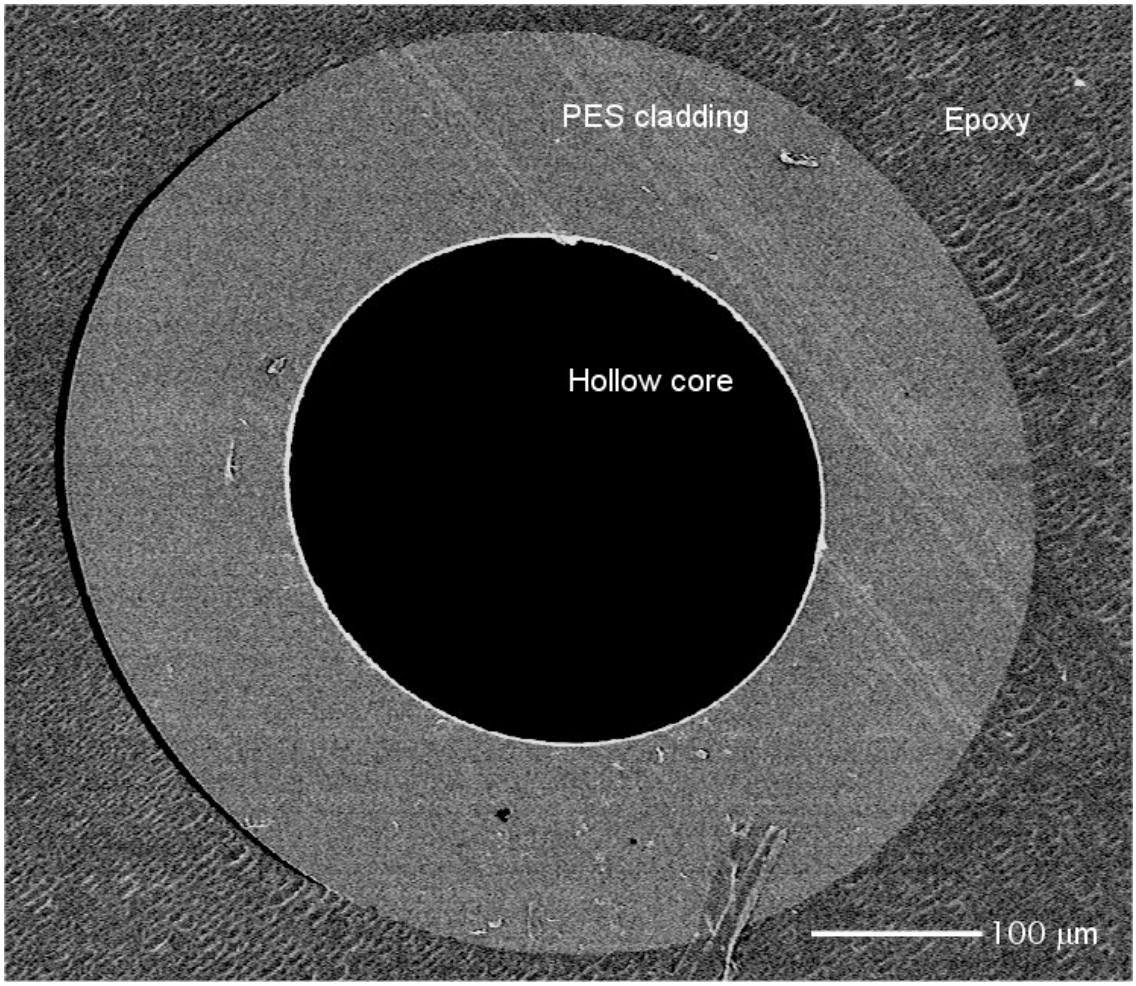

Fig.1 Cross-sectional SEM micrographs of a 509-μm-OD fiber with a fundamental photonic bandgap at a wavelength of 0.85 μm mounted in epoxy are shown in (A), with multilayer structure lining around hollow core; (B) demonstrates that the multilayer structure adheres well to a thin layer of PEI, and the PEI layer does to a thick layers of PES as well; (C) reveals the ordering of alternating layers with As_2Se_3 (bright layers), and PEI (grey layers). The PEI layers have a thickness of 200 nm, and the As_2Se_3 layers are 60-nm-thick (except for the first and last As_2Se_3 layers, which are 30 nm).

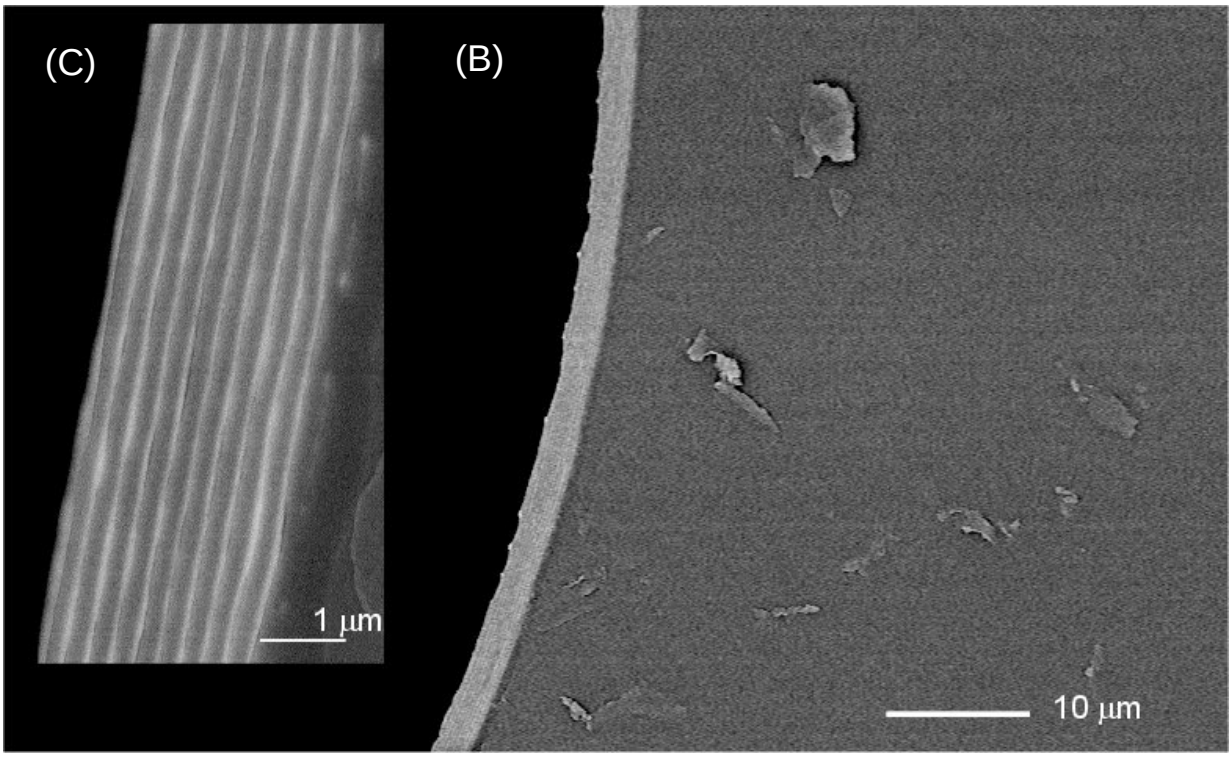
(C)
(B)
1 μm
10 μm

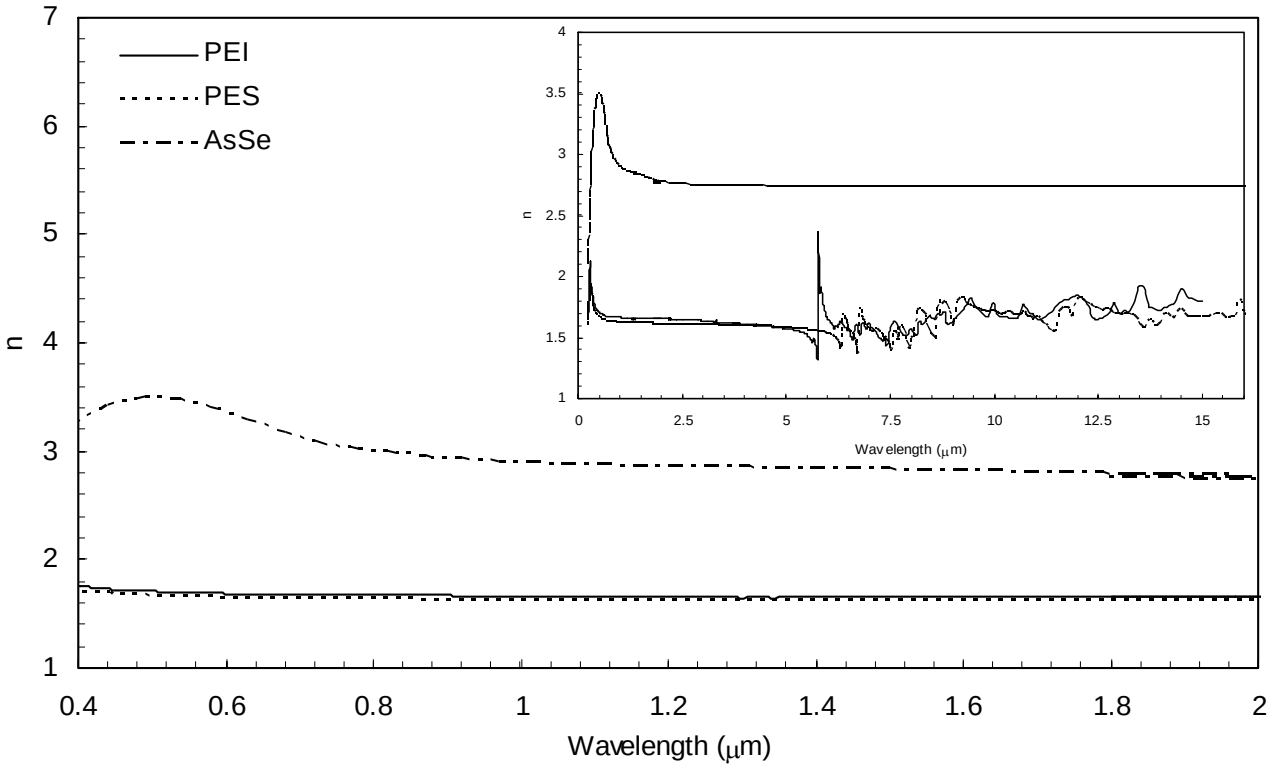

Fig.2
Refractive indices of As_2Se_3, PEI and PES measured by spectroscopic ellipsometry. The As_2Se_3 has a large change from 400 nm to 2 μm due to its material electronic band-gap around 3 eV. The inset shows refractive indices of those up to 15 μm. The polymeric materials have a lot of vibrational absorption from 5 μm to 15 μm.

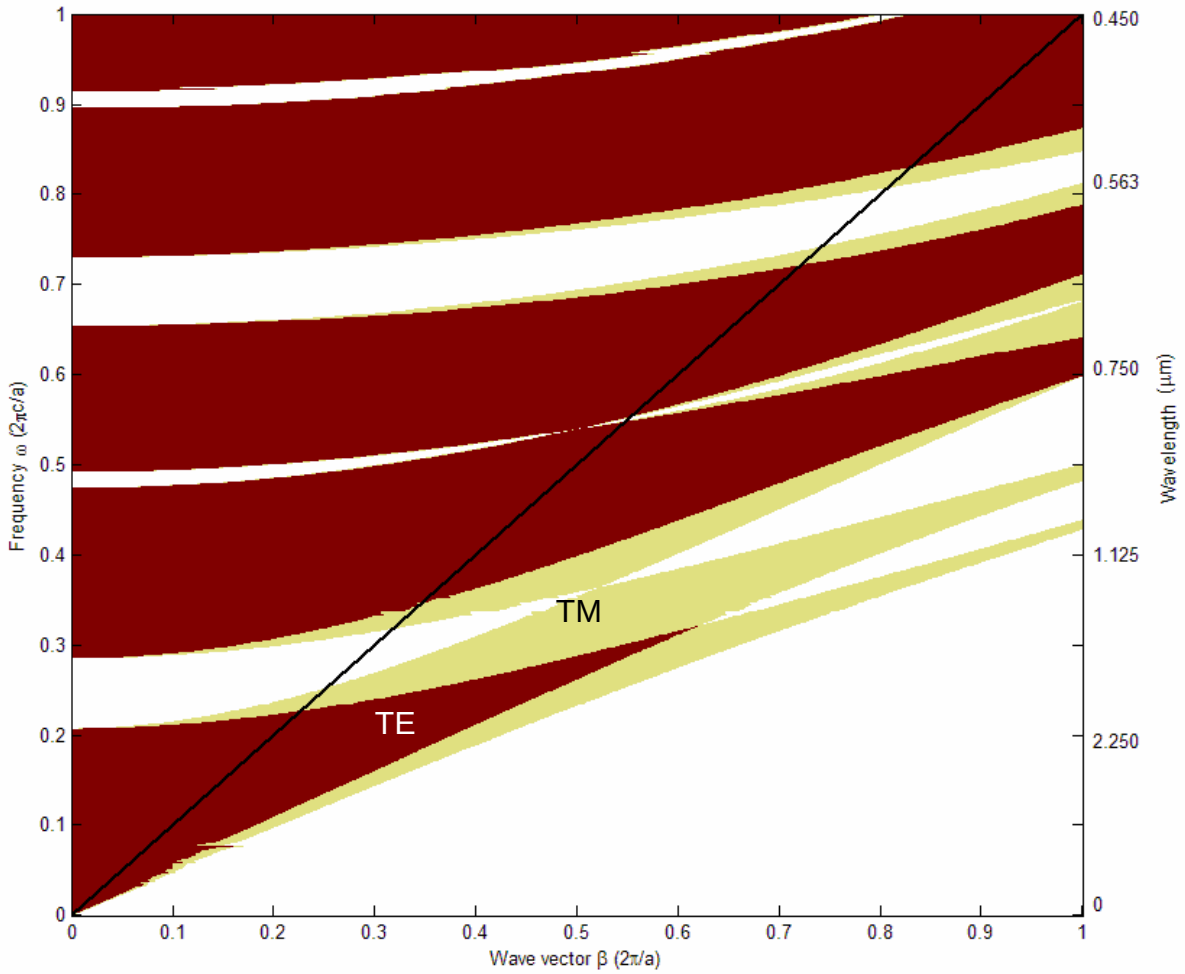

Fig.3
Calculated photonic band diagram for a one dimensional photonic crystal having a periodic refractive index alternating between As_2Se_3 and PEI. The black and grey regions represent modes radiating thorough the multilayer structures for both the TE and TM modes, and only TM, respectively. Modes propagating through air and reflected by the fiber walls lie in the bandgaps (white) and above the light cone defined by the glancing-angle condition (black line). Pure TE modes can be confined more than pure TM modes. Parameters used in this calculation were experimentally obtained; the refractive indices from ellipsometry (Fig. 2) and the layer thicknesses from SEM inspection. The layer thicknesses of As_2Se_3 and PEI were 100 nm and 350 nm, respectively, corresponding to the measured fiber with a fundamental bandgap at ~1.55 μm.

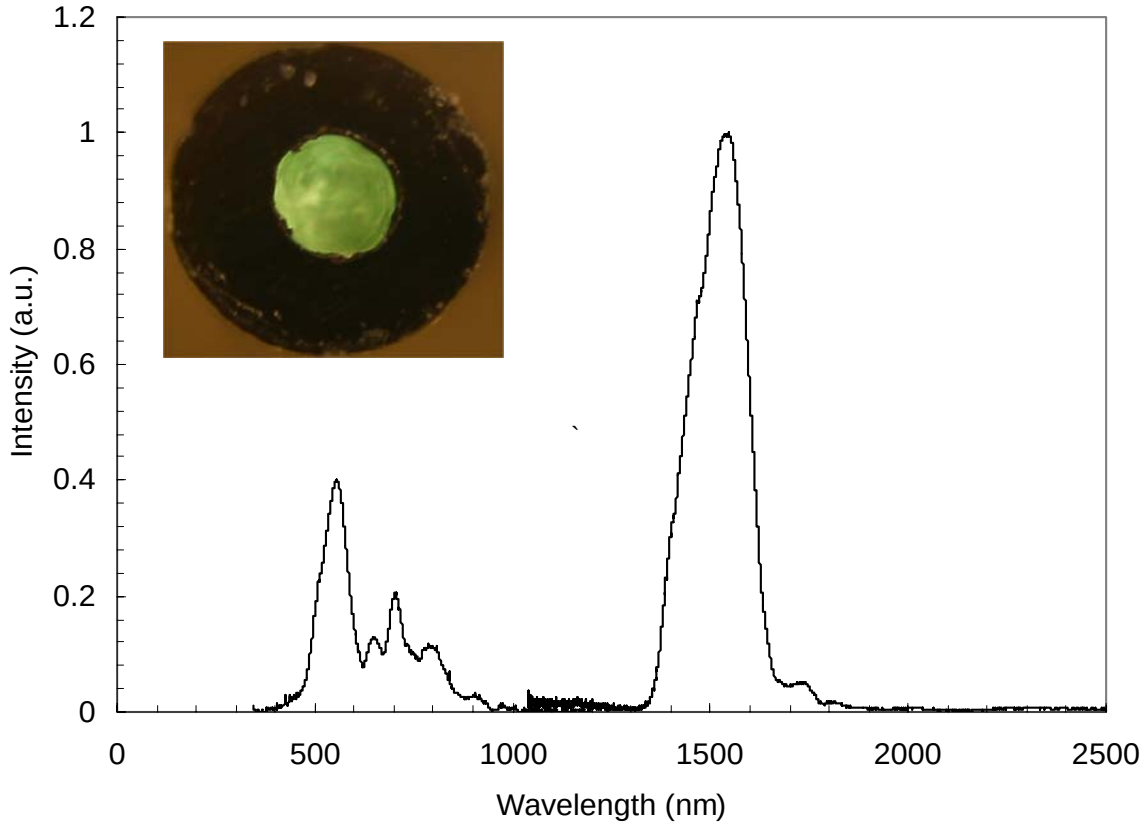

Fig.4
Transmission spectra for a hollow-core photonic bandgap fiber. The fundamental photonic bandgap is centered at 1.55 μm measured with FTIR, and the third-order gap is around 560 nm with spectrum analyzer. Inset is an optical micrograph of the field intensity pattern corresponding to the third-order band gap at the exit face of the fiber excited by a QTH light at the entrance face. The measured fiber has a hollow-core diameter of 241 μm.

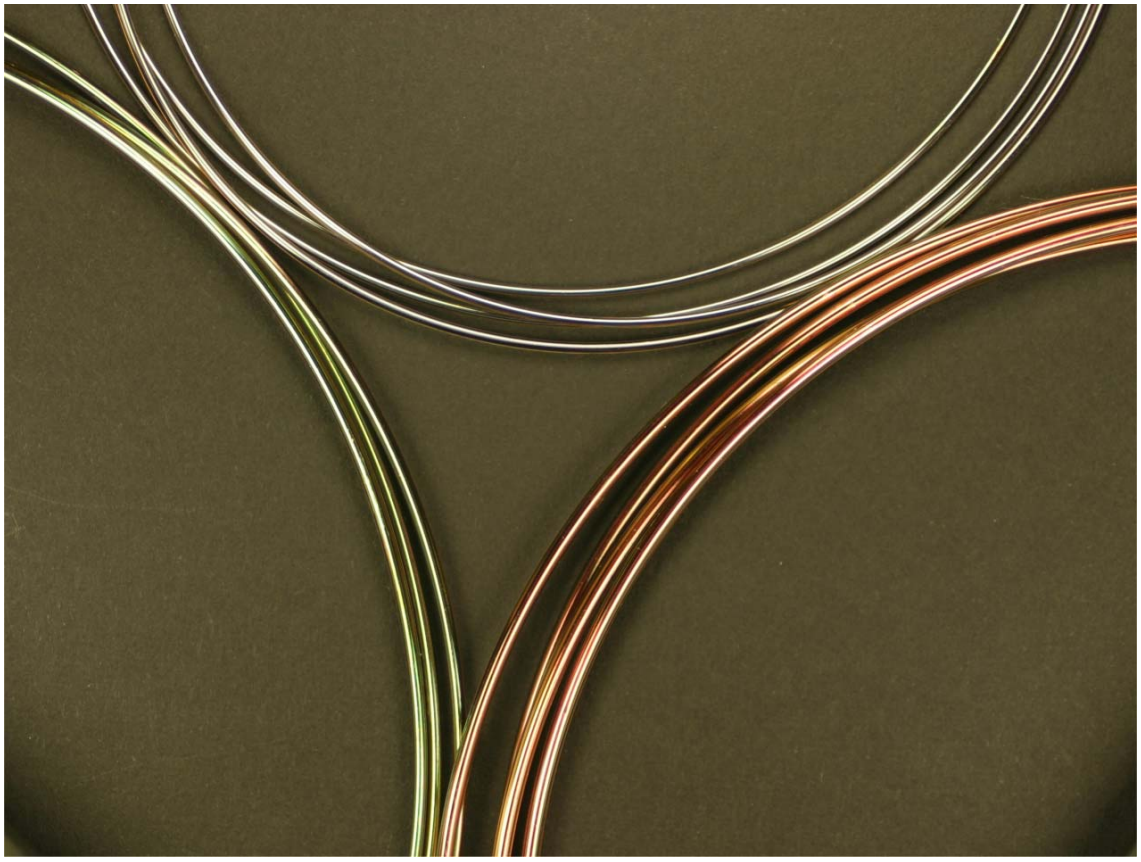

Fig.5
Coiled fibers made from 1,218-μm-OD (red), 1,013-μm-OD (green), and 621-μm-OD (blue) fibers used to obtained transmission data in Fig.7.

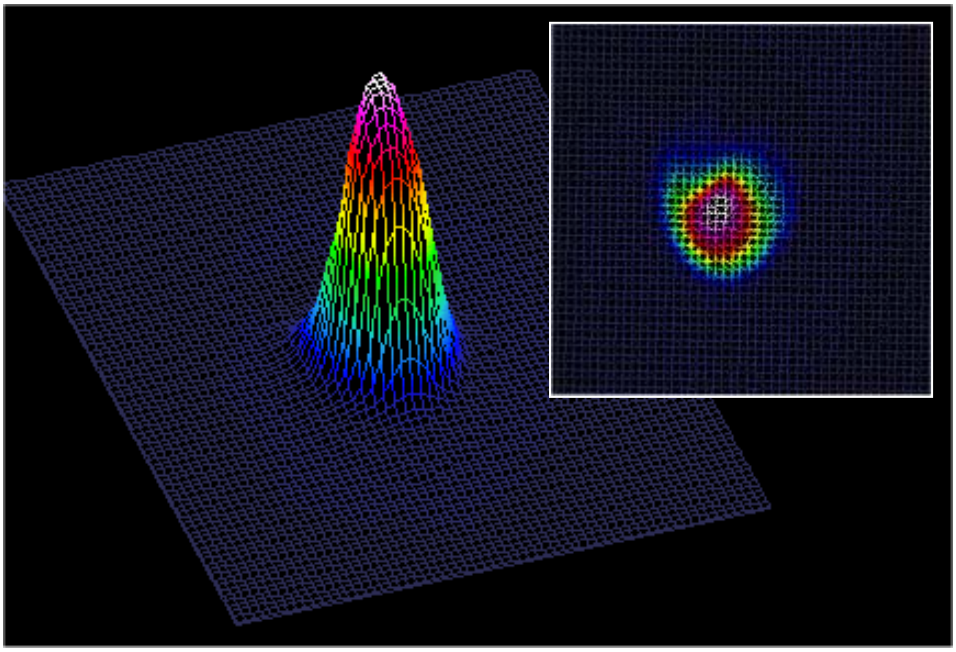

Fig.6
Output field pattern of a QTH light from a hollow-core photonic bandgap fiber held nominally straight. The fiber was 30 cm long, and the fiber hollow core is 241 μm.

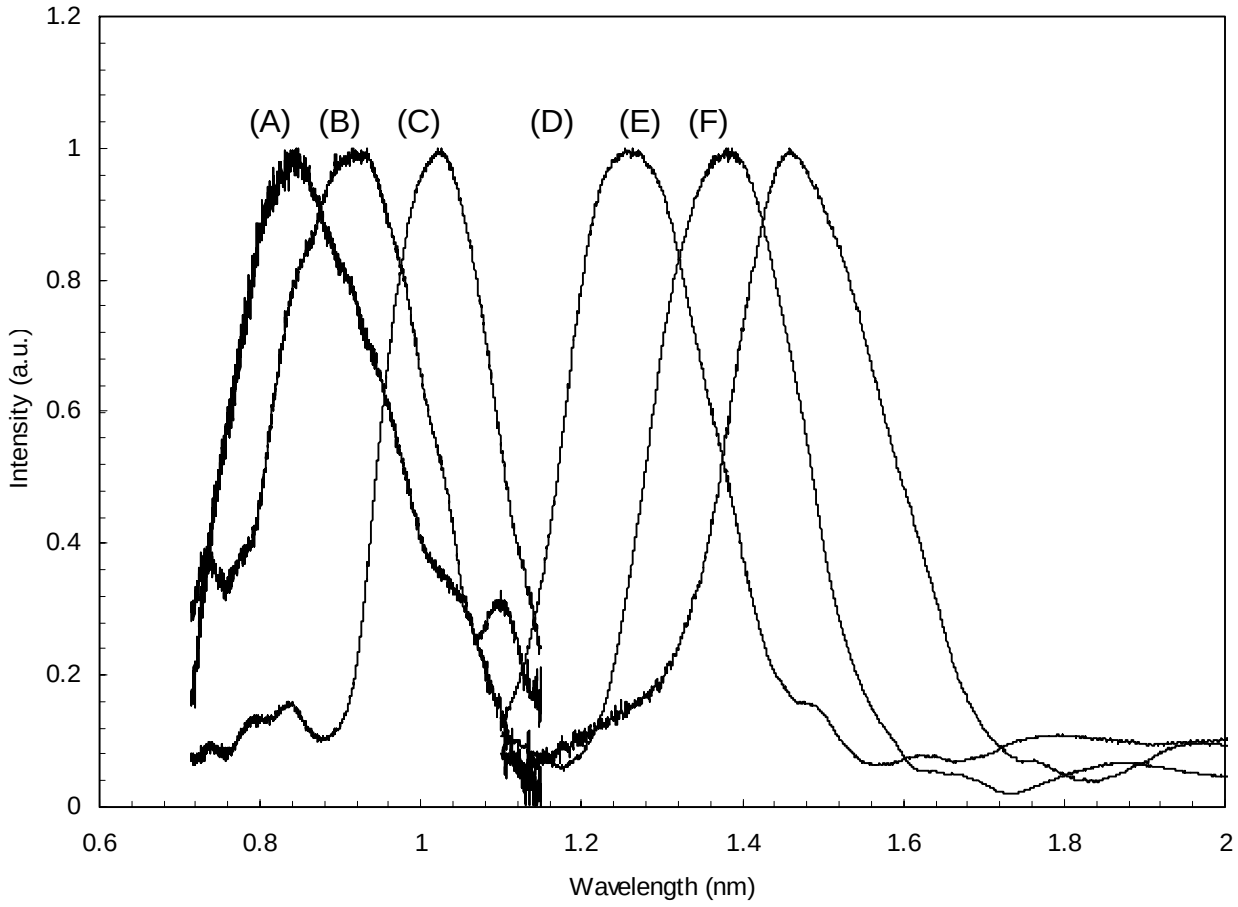

Fig 7
Measured normalized transmission spectra for (A) 1,218-μm-OD, (B) 1,094-μm-OD, (C) 1,013-μm-OD, (D) 783-μm-OD, (E) 621 -μm-OD, (F) 509-μm-OD hollow-core photonic bandgap fibers. The fundamental photonic bandgaps are centered from 0.85 to 1.47 μm. Peak wavelengths from (A) to (F) are 1.47, 1.39, 1.27, 1.03, 1.93 and 0.85 μm, respectively.

Appendix D.

Layout of Quantum Interference through PBG fiber Experiemnt

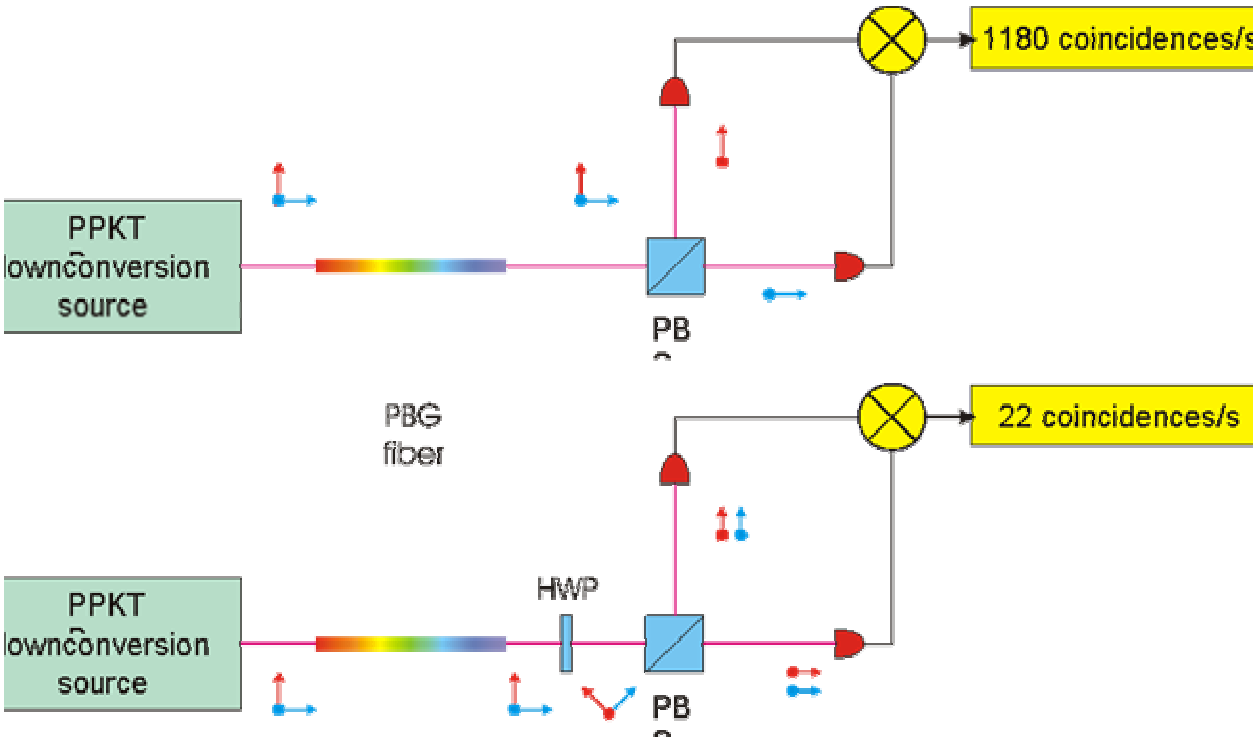

Quantum interference visibility of 96% (~ same as without the PBG fiber)

We expect to be able to transfer entanglement with high fidelity

Appendix E:

Efficient Fiber Eigenmode Coupling Via Spatial Phase Modulator

Abstract

The objective of this project is to demonstrate the feasibility of low-loss optical communication over our recently developed OmniGuide optical fibers over a wide range of wavelengths using specially designed spatial optical modes. These modes are the eigenmodes of OmniGuide fibers, and their special features are a result of the unique electromagnetic boundary conditions enforced by the multilayer structure surrounding the hollow core of the fiber. The mode with the lowest expected loss in the fiber is the transverse electric mode TE_{01}, in close analogy to the case of metallic waveguides.

The results of this research are expected to lead to the development of novel OmniGuide-fiber-based communication links and optoelectronic devices. The understanding of the propagation characteristics of the eigenmodes of the fiber will give us a better understanding of the performance of the fibers and any necessary changes needed in our developed fabrication process. Since these fibers have a hollow core, we expect low material losses (due mainly to the cladding materials). The ability to produce and test the propagation of any required mode will enable us to identify the mode with the lowest loss and further study its characteristics.

The device we are requesting is a spatial light modulator, which imparts a spatially varying phase to an incident optical wave front, that has specially designed features not provided in commercially available devices. We require a device that operates in a dual band mode, in other words, a device that is capable of performing reliable spatial light modulation in two different wavelength bands, namely the 800-900-nm band and the 1.4-1.6-μm band. This requires redesigning parts of the device and recalibration of the optical phase imparted to the incident wave front for both bands. This device will be incorporated into an optical setup where the required optical modes are generated and coupled into our fibers. We intend to measure the loss and dispersion characteristics of these modes and intermode coupling, which lends a more complete characterization than has been hitherto achieved for a photonic bandgap fiber.

We propose the synthesis of novel optical spatial modes that are *eigenmodes* of the OmniGuide optical fibers that our laboratory has pioneered and developed. OmniGuide fibers can be considered a member of the family of photonic crystal fibers, a field that has generated a lot of interest of late and promises to initiate a renaissance of research on optical fibers and devices.

What sets our OmniGuide fibers apart from other photonic crystal fibers is that (1) our fibers are completely cylindrically symmetric, and that (2) they rely on material systems that are uniquely distinct from silica, the sole material that has been used by all other groups to date. The fibers consist of a cladding of alternating layers of two materials (with large index-of-refraction contrast and sub-micrometer thickness) surrounding a hollow core. Light is then guided in this hollow core by Bragg reflection from the multilayer cladding. The cladding may be considered a one-dimensional photonic crystal that features a complete photonic bandgap, i.e., light incident from all directions and all polarizations is reflected. The center wavelength and bandwidth are controlled via design of the parameters of the material parameters of the multilayers and the

dimensions of the structure. As a result, light in the specified photonic bandgap is guided along the fiber.

We have recently demonstrated the design, fabrication, and operation of such fibers [1]. We have furthermore observed light propagation due to higher order bandgaps (i.e., at short wavelengths).The aim of utilizing both original and higher order bandgaps is a further motivation for applying to the PTAP for this device.

Since the mechanism that results in the propagation of light in OmniGuide fibers is distinctly different from that in conventional optical fibers (where light is guided by total internal reflection), we expect that the spatial modes to also be different. We have carried out extensive research on this question [2]. The modes of lowest loss in these fibers are the transverse electric (TE) modes. These modes have characteristic spatial amplitude, phase, and polarization distributions that are uncommon to practitioners of fiber optics. These modes are, in fact, very similar to the modes of metallic waveguides, a feature unique to our fibers because of the special boundary conditions imposed on the optical fields at the cladding. Other modes of interest are the transverse magnetic (TM) modes, and hybrid modes (EH and HE).

These modes (TE and TM) are quite common in microwave physics where they are easily generated. However, to the best of our knowledge, these modes have not been previously observed at optical wavelengths, where an application has not previously arisen for them. We propose in what follows a procedure to produce such modes.

Consider, for simplicity, the TE_{01} mode, whose intensity and polarization vector distribution and is depicted in Fig. 1. Such a beam, when analyzed by a polarized beam splitter, yields *x*- and *y*-polarized beams, with amplitude and phase distributions shown in Fig. 1(b). Generation of the TE_{01} mode thus rests on the possibility of producing these two linearly polarized beams and the superposition of them thereon. An optical system that performs such a task is shown in Fig. 2. The optical element of the most importance in this setup, and the core of this proposal is the spatial light modulator (phase modulator).

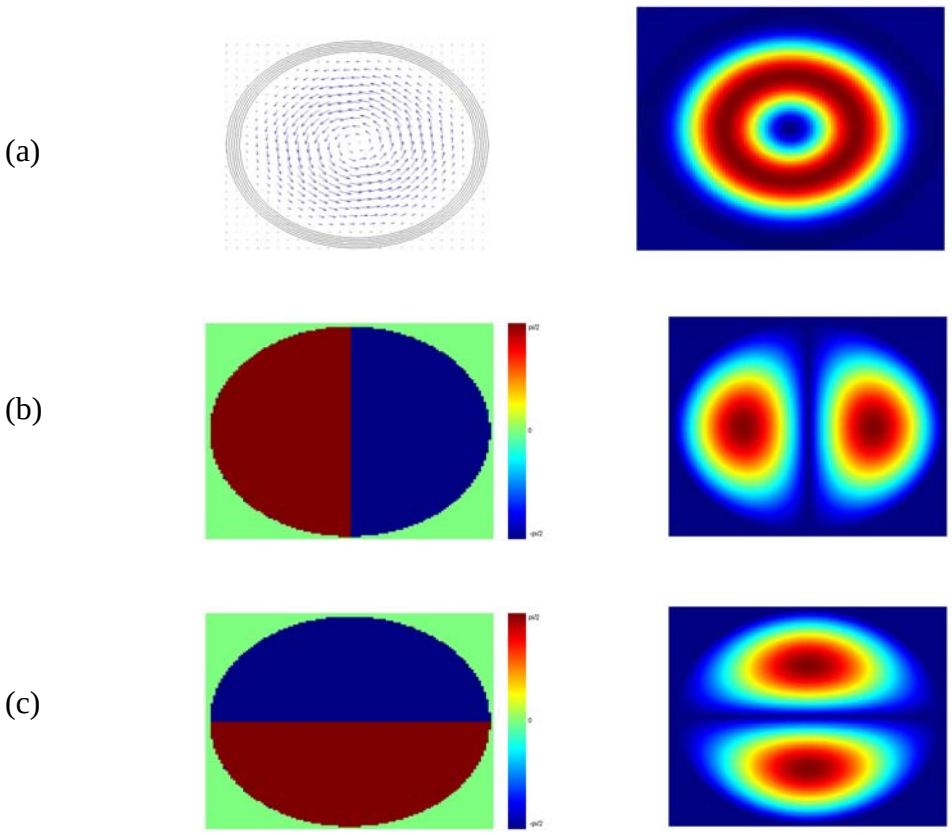

Figure 1 (a) Amplitude distribution (right) and polarization direction (left) of the electrical field of the TE_{01} mode. (b) Phase (left) and amplitude (right) distributions of the TE_{01} *x*-polarized component, while (c) shows the same for the *y*-polarized component of the mode.

The proposed optical setup makes use of the concatenation of two optical devices: an amplitude modulator (micro-mirrors array, such as those commonly used in projector displays) and a phase modulator (a programmable phase modulator (PPM), such as that produced by Hamamatsu). The conjunction of both the amplitude and phase modulating device will be used to produce the complex field distribution of the *x*-polarization component. The *y*-polarized component is a spatially rotated version of the *x*-polarized component. One can achieve such a rotation in several ways. One simple example is to use a dove prism that is rotated around its axis.

These devices are commonly designed to be used in the visible spectrum and they have played a major role in the recent advances in the field of optical tweezers [3]. The expected price of this item is approximately $32,000, based on an estimate by the company (Hamamatsu) representative.

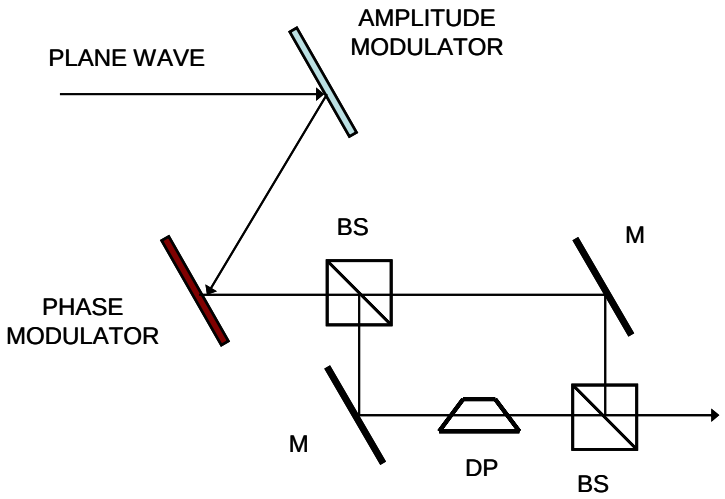

Figure 2 Schematic of optical setup to produce transverse-electrical optical fields. A plane wave illuminates an amplitude modulator and then a phase modulator that produces a required wave front. The modulated scalar beam enters a specially designed Mach-Zhender interferometer to produce the required vector beam.

In Fig. 2 we show the optical setup to produce TE modes. A linearly polarized (*x*, for example) plane wave illuminates the amplitude modulator (with the required amplitude distribution encoded on it), and the resulting beam is then directed to the phase modulating device (programmable phase modulator, PPM). The modulated beam is then split into two halves that travel along the two arms of a Mach-Zhender (MZ) interferometer. In one of the arms of the MZ interferometer a dove prism (or any other spatially rotating device) is placed so as to rotate the beam by 90º, resulting in a *y*-polarized beam. The two beams are then combined at the output of the MZ interferometer beam splitter yielding the required electric field distribution. This beam is directed to an optical minification system and is coupled to the OmniGuide fiber.

We have a fully developed optical laboratory, equipped with three optical tables, several laser systems (CW Argon, femto/picosecond Ti:Sa, Verdi, Tunable laser diode module,..) and several advanced optical characterization devices (FTIR spectrometer, spectroscopic ellipsometer,..). We have several beam visualization devices that cover the visible, NIR, and MIR bands of the optical spectrum. We also have access to several shared facilities at MIT that enable us to use a wide range of optical characterization equipment.

References

[1] B. Temelkuran, S. D. Hart, G. Benoit, J. D. Joannopoulos, Y. Fink, *Nature* **420**, 650-653 (2002); S. D. Hart, G. R. Maskaly, B. Temelkuran, P. H. Prideaux, J. D. Joannopoulos, Y. Fink, *Science* **296**, 511-513 (2002).

[2] T. D. Engeness, M. Ibanescu, S. G. Johnson, O. Weisberg, M. Skorobogatiy, S. Jacobs, and Y. Fink, *Opt. Express* **11**, 1175-1198 (2003); Mihai Ibanescu, Steven G. Johnson, Marin Soljacic, J. D. Joannopoulos, Yoel Fink, Ori Weisberg, Torkel D. Engeness, Steven A. Jacobs, and M. Skorobogatiy, *Phys. Rev. E* **67**, 046608 (2003).

[3] David G. Grier, *Nature* **424**, 810 - 816 (2003).

Appendix F:

METAL INSULATOR SEMICONDUCTOR OPTOELECTRONIC FIBRES

Mehmet Bayindir,[1] Fabien Sorin,[2,3*] Ayman F. Abouraddy,[1*] Jeff Viens,[1,3] Shandon D. Hart,[1,3] John D. Joannopoulos,[1,2,4] and Yoel Fink[1,2,3**]

[1]Research Laboratory of Electronics, [2]Center for Materials Science and Engineering, [3]Department of Materials Science and Engineering, [4]Department of Physics Massachusetts Institute of Technology, Cambridge, MA 02139, USA.

[*] These authors contributed equally to this work

[**]To whom correspondence should be addressed: yoel@mit.edu

The combination of conductors, semiconductors, and insulators in well-defined geometries and prescribed sizes while forming intimate interfaces, is essential to the realization of practically all functional electronic and optoelectronic devices. These are typically produced using a variety of elaborate wafer-based processes, which afford small features, but are restricted to planar geometries and limited coverage area [1-3]. Preform-based fibre-drawing techniques are, in comparison, simpler, yield extended lengths of highly uniform fibre having well controlled geometries and excellent optical transport characteristics [4], but have been restricted to particular materials [5-7] and larger features [8-12]. Here we report on the design and fabrication of fibres made of conducting, semiconducting, and insulating materials in intimate contact and in a variety of geometries. A tunable fibre photodetector comprising an amorphous semiconductor core contacted by metallic micro-wires, and surrounded by a cylindrical-shell resonant optical cavity, is thermally drawn from a macroscopic preform. Each fibre is sensitive to illumination along its entire length (10's of meters) thus forming a photodetecting element of dimensionality one. A fabric, capable of performing illumination detection on large areas with only order *N* number of elements (in contrast to the conventional order N^2 in zero-dimensional

detectors) is woven from the photodetecting fibres. The ability to interface materials with widely disparate electrical and optical properties in a fibre, achieve submicron features, and realize arbitrary geometries over extended fibre lengths, presents the opportunity to deliver novel semiconductor device functionalities at fibre-optic length scales and cost.

Our approach entails the drawing of extended fibre lengths fabricated by arranging a low-melting temperature crystalline conductor (Sn), amorphous semiconductors (As-Se-Te-Sn and As_2Se_3), and high glass-transition-temperature polymeric insulators (polyetherimide, PEI, and polyethersulfone, PES) into a preform which shares the final fibre geometry but lacks functionality due to the absence of intimate contact and proper element dimensions. The preform is subsequently heated and drawn into a fibre which preserves the initial geometry while forming intimate interfaces and feature sizes down to below 100 nm. This process has led to the creation of two prototypical functional fibre structures that we discuss in detail in this letter: 1) a fibre designed for dual electron-photon transport, and 2) a tunable narrow band fibre photodetector.

The fibre for dual electron-photon transport is comprised of a hollow air core, surrounded by an omnidirectional dielectric mirror [13-17] formed from 8 pairs of alternating layers of As_2Se_3 and PEI (layer thicknesses of 150 and 280 nm, respectively). The refractive indices of As_2Se_3 and PEI are 2.83 and 1.65 respectively at 1.5 μm as measured by using a Sopra GES5 UV-Vis-IR spectroscopic ellipsometer [18]. This multilayer structure provides the optical confinement to the low index core. Immediately adjacent to this omnidirectional mirror is a circular array of 60 Sn metal wires with diameters of ~8 μm each (see Methods, Fibre fabrication). The whole fibre is then surrounded with a PES polymer cladding. An SEM micrograph of the fibre cross section is shown in Fig. 1A. The optical transport characteristics of the fibre are determined by the positions of the photonic bandgaps. For example, fibres having outer diameters of 980, 1030, and 1090 μm have fundamental bandgaps centered at 1.62, 1.75, and 1.85-μm wavelengths, respectively (see Fig. 1C). Optical transmission spectra were determined using an FTIR

spectrometer (Bruker Tensor 37). The fibre shown in Fig. 1B (1-mm outer diameter) appears green to the eye because of reflection from the third-order bandgap.

We have carefully investigated the losses incurred upon propagation through *simple* hollow-core multilayer photonic bandgap fibres in Refs. [15-17]. The loss of such fibres for radiation at a wavelength of 10.6 μm was found to be less than 1 dB/m [17]. More recently, we have characterized such fibres at a wavelength of 1.5 μm, and the loss was found to be approximately 5.5 dB/m [15]. The loss mechanisms are found to be (1) radiation through the multilayers; (2) intrinsic materials absorption; (3) nonuniformity in the layer thicknesses; (4) and scattering due to internal surface roughness. These losses, while being higher than those for silica-based holey fibres, are among the lowest reported values for hollow polymer fibers. As the light in the electron-photon fibre is very strongly confined within the hollow core by the cylindrical omnidirectional mirror it is expected that the presence of additional material components or structural complexity lying *outside* of the cylindrical mirror will not significantly affect the losses through this hollow fibre. Initial loss measurements on the electron-photon conducting fibres yield loss levels that are comparable to the cylindrical photonic bandgap fibres of similar structural characteristics. In order to examine the electrical properties of the fibre, on the other hand, both ends of the fibre were coated with a thick layer of gold that electrically connects all the Sn wires. The current-voltage characteristics of the 980-μm thick fibre are displayed in Fig. 1D, showing clear ohmic response.

Whereas the above fibre exhibits both electrical and optical *transmission* properties, these are spatially separated and independent, i.e., the propagating electrons and photons do not interact. In our second fibre, we specifically introduce an optoelectronic *interaction*. This is realized by forming, in the core of the fibre, a photoconductive chalcogenide cylinder contacted with metal electrodes that produces current upon illumination under bias conditions. A single (radial) mode cylindrical-shell optical cavity is introduced in the optical path shielding the photoconducting core from ambient illumination sources. Upon *external* illumination, when the wavelength of the

radiation matches that of the cavity resonance, we observe an electric response from the fibre core thus establishing the *spectroscopic* functionality of the fibre.

Figure 2 shows SEM micrographs of the spectroscopic fibre cross-section. The fibre core is $As_{40}Se_{50}Te_{10}Sn_5$ highly photoconductive (AST-Sn) glass optimized subject to the following requirements (see Methods, Glass preparation): (1) large photoconductivity in the measurement range; (2) viscosity range compatible with the polymer; and (3) enhanced stability against crystallization during fibre drawing. The core is contacted by four Sn electrodes to form the photodetecting element. An enlargement of the metal-semiconductor interface demonstrating the intimate contact is shown in Fig.2A. A resonant optical cavity structure is formed by a multilayer made of As_2Se_3 and PEI with a $\lambda/2$ defect layer, an enlargement of the resonant cavity structure is shown in Fig 2B. The micrograph shown in Fig. 2C demonstrates excellent contact between the semiconducting core and a metal electrode (see Methods, Fibre fabrication).

In order to confirm the fidelity of the metal-semiconductor contact and characterize its photoconductive properties, we measured the broad-band photoconductive response of a two-electrode fibre without a multilayer structure (the red curve in Fig. 3A). A 50-volt DC voltage was applied to the fibre and the current was measured using a pico-ampere meter / DC voltage source (Yokogawa / Hewlett Packard 4140B). The fibre is illuminated externally with a laser beam from a tunable Optical Parametric Oscillator (OPO). Optical transmission of bulk glass (12-mm diameter and 5-mm length) was determined by an FTIR measurement (blue curve in Fig. 3A). The spectral photoconductive response is commensurate with the optical transmission measurement.

The resonance wavelength and photonic band gap are both determined by the device fibre outer diameter. We fabricated three fibres of outer diameters 870, 890, and 920 μm, which have calculated resonance wavelengths of 1.26, 1.29, and 1.33 μm, respectively. In these fibres, the multilayer structure was situated at the fibre outer surface. The multilayer structure in the three

fibres consists of 3 bilayers, As_2Se_3 and PEI, a $\lambda/2$ PEI cavity, followed by three more bilayers. For the 920-μm fibre, for example, the thicknesses of As_2Se_3 and PEI layers are 117 and 204 nm, respectively. The reflectivity of the optical cavity structure was measured for single fibres having these diameters with an FTIR spectrometer (Nicolet/SpectraTech NicPlan infrared microscope and Fourier transform infrared spectrometer [Magna 860]), and are displayed in Fig. 3B. The FTIR spectra agree well with the calculated spectra. Since the microscope objective admits a range of angles that vary from normal incidence to 35^o, the observed dip in the reflection spectra is wider and shallower. The cavity resonance shifts slightly in wavelength when the angle of incidence changes. Such a large angular cone, as determined by the microscope objective numerical aperture (NA) of 0.58, leads to an averaging effect that reduces the apparent quality factor of the cavity mode.

In order to characterize the optoelectronic response of our integrated device fibre, it is useful to measure both the electrical photocurrent and optical reflectivity simultaneously. We externally illuminated the three aforementioned two-electrode device fibres with the OPO laser beam and measured the back-reflected light though a beam splitter, while simultaneously monitoring the generated photocurrent (see Methods, Optical characterization of device fibre).

In Fig. 3C, we display the measurement results of the back-reflected light from three different fibres as wavelength of the laser beam is swept. Concurrently, in Fig. 3D we plot the results of photocurrent measurements of these fibres. At the resonance wavelength, the back-reflection is diminished, and the light reaches the photoconductive core. Consequently, the corresponding photocurrent is enhanced.

These novel fibre structures offer a unique possibility for constructing an *optoelectronic functional fabric* since the fibres are both flexible and mechanically tough, and thus can be woven, as shown in Fig. 4. The fibres chosen to be used in this fabric are of slightly different diameters (400-500 μm), and hence exhibit different bandgap positions, and resonant cavity

wavelengths, manifested in their colors (corresponding to higher order photonic bandgaps). Furthermore, interesting device applications follow not only from the ability to engineer the single fibre properties, but also from the specifics of fibre arrangements into larger assemblies. For example, in constructing a two-dimensional optical detector array, a desired resolution of $N \times N$ pixels per unit area would require N^2 point (dimensionality zero) detection elements. A woven fabric, on the other hand, provides a grid structure, out of linear (one-dimensional) fibres, which in turn can be used to localize an illumination point on a surface but with *only order N* detection elements. Moreover, by overlapping layers of this fabric, one could even ascertain the *direction* of incoming illumination. These fibres thus enable the realization of large-area optoelectronic functional surfaces.

Methods

Fibre fabrication

Dual electron-photon transport fibre: Metal-core polymer-cladding fibres were drawn from a preform with 5 mm Sn (99.75% purity) core and 7.5 mm PES cladding. The preform was consolidated in a vacuum oven at 260^o C, and then drawn at ~305^o C in a vertical tube furnace. Both ends of the preform were closed with polymer to confine the metal during consolidation and drawing processes. Meters of uniform metallic fibres with outer diameters from 500 μm to 1.2 mm were successfully drawn. Sixty of these fibres were used in the construction of a macroscopic preform that yields the current hybrid fibre after drawing.

Spectroscopic fibre: These fibres were drawn in a three-zone vertical tube furnace at a temperature of 300^{o}C at speeds ranging from 0.7 to 3 m/min.

Glass preparation

The amorphous semiconductor glass, $As_{40}Se_{50}Te_{10}Sn_5$, is prepared from high purity As, Se, Te, and Sn elements using sealed-ampoule melt quenching techniques. The materials were weighed and placed into a quartz tube under a nitrogen atmosphere. The tube was heated to 330^o C for an hour at a rate of 1^o C/min under vacuum to remove surface oxide, and cooled to room

temperature at a same rate. The ampoule was formed by sealing the tube under vacuum (~10^{-5} Torr). It was then heated to 800^{o} C at a rate of 2^{o} C/min in a rocking furnace, while held vertical, for 24 hours and then rocked for 6 hours in order to increase mixing and homogenization. The glass liquid was cooled to 600^{o} C in the furnace, and then quenched in water. Subsequently, it was annealed for half an hour near to glass transition temperature, T_g=180^{o} C, before being cooled gradually to room temperature. Using this procedure, mechanically strong glass rods with diameter 12 mm and length 18 cm were obtained.

Optical characterization of device fibre

For optical characterization, we used a Verdi10 (Coherent) to pump a Ti-S femtosecond laser (Mira 900, Coherent). The femtosecond laser beam was then down converted using an OPO (Mira OPO, Coherent). The OPO beam size was adjusted using a pinhole before passing through a beam splitter to allow collection of back-reflected light from the fibre. The beam emerging from the beam splitter was focused onto the outer surface of the fibre using a ×5 microscope objective (NA 0.1). The optical power incident on the fibre surface was maintained at 30 mW, using a variable optical attenuator, while the wavelength of the laser beam was swept. Back-reflected light through the beam splitter was detected using a Newport InGaAs photodetector model 818-IG. For simultaneous electrical characterization, we measured the current flowing through the fibre electrodes using a pico-ampere meter / DC voltage source (Yokogawa / Hewlett Packard 4140B). The DC voltage difference applied to the two fibre electrodes was 50 volts. At each wavelength, the incident optical power was adjusted, the electrical current was recorded, and the back-reflected light power measured.

REFERENCES

[1] Sze, S. M. *Semiconductor Devices: Physics and Technology* (John Wiley, 2nd Ed., 2001).

[2] Sedra, A. S. & C. S. Kenneth *Microelectronic Circuits* (Oxford University Press, 2003).

[3] Chuang, S. L. Physics *of Optoelectronic Devices* (John Wiley, 1995).

[4] Sanghera, J. S & Aggarwal, I. D. Eds., *Infrared Fiber Optics* (CRC Press, New York, 1998).

[5] Harrington J. A. A review of IR transmitting, hollow waveguides, *Fiber Integr. Opt.* **19**, 211-227 (2000).

[6] Katagiri T., Matsuura, Y. & Miyagi, M. Metal-covered photonic bandgap multilayer for infrared hollow waveguides, *Appl. Opt.* **41**, 7603-7606 (2002).

[7] Large, M. et al. Microstructured optical fibers: Why use polymers? Proc. 29th Eur. Conf. on Opt. Comm. (ECOC'03 Rimini), 1014-1017 (2003).

[8] Broeng, J., Mogilevstev, D., Barkou, S. E. & Bjarklev, A. Photonic crystal fibers: A new class of optical waveguides, *Opt. Fiber Technol.* **5**, 305-330 (1999).

[9] Eggleton, B. J., Kerbage, C., Westbrook, P. S., Windeler, R. S. & Hale, A. Microstructured optical fiber devices, *Opt. Express* **9**, 698-713 (2001).

[10] van Eijkelenborg, M. A. *et al*. Microstructured polymer optical fiber, *Opt. Express* **9**, 319-327 (2001).

[11] Allan, D. C. *et al.*, in *Photonic Crystal and Light Localisation in the 21st Century*, C. M. Soukoulis, Ed. (Kluwer Academic, Dordrecht, Netherlands, 2001), pp. 305–320 (2002).

[12] Knight, J. C. Photonic crystal fibres, *Nature* **424**, 847-851 (2003).

[13] Yeh, P., Yariv, A. & Marom, E. Theory of Bragg fiber, *J. Opt. Soc. Am.* **68**, 1196-1201 (1978).

[14] Fink, Y. *et al.* A Dielectric omnidirectional reflector, *Science* **282**, 1679-1682 (1998).

[15] Kuriki, K. *et al.* Hollow multilayer photonic bandgap fibers for NIR applications, *Opt. Express* **12**, 1510-1517 (2004).

[16] Hart, S. D. *et al.* External reflection from omnidirectional dielectric mirror fibers, *Science* **296**, 510-513 (2002).

[17] Temelkuran, B., Hart, S. D., Benoit, G., Joannopoulos, J. D. & Fink, Y. Wavelength-scalable hollow optical fibres with large photonic bandgaps for CO_2 laser transmission, *Nature* **420**, 650-653 (2002).

[18] The refractive indices of the materials used in this paper, measured by a Sopra GES5 UV-Vis-IR spectroscopic ellipsometer, is available online at: http://mit-pbg.mit.edu/Pages/Ellipsometry.html.

Mehmet Bayindir's e-mail address is *mehmet@mit.edu*. MB thanks P. H. Prideaux for teaching him the ways of optical fibre drawing. We also thank G. Benoit for measuring refractive indices of As_2Se_3 and PEI, N. Orf for measuring the glass transition temperature of chalcogenide glasses, Y. Kuriki for taking SEM micrographs, and K. Kuriki for providing PEI polymer film. This work was supported in part by DARPA/Carrano and DARPA/Griggs, DARPA QUIST, the ARO, the ONR, the AFOSR HEL-MURI, the US DOE, the ISN and an NSF Graduate Research Fellowship. This work was also supported by the Materials Research Science and Engineering Center (MRSEC) program of the NSF and made use of the Shared Experimental Facilities supported in part by the MRSEC Program of the NSF

FIGURES

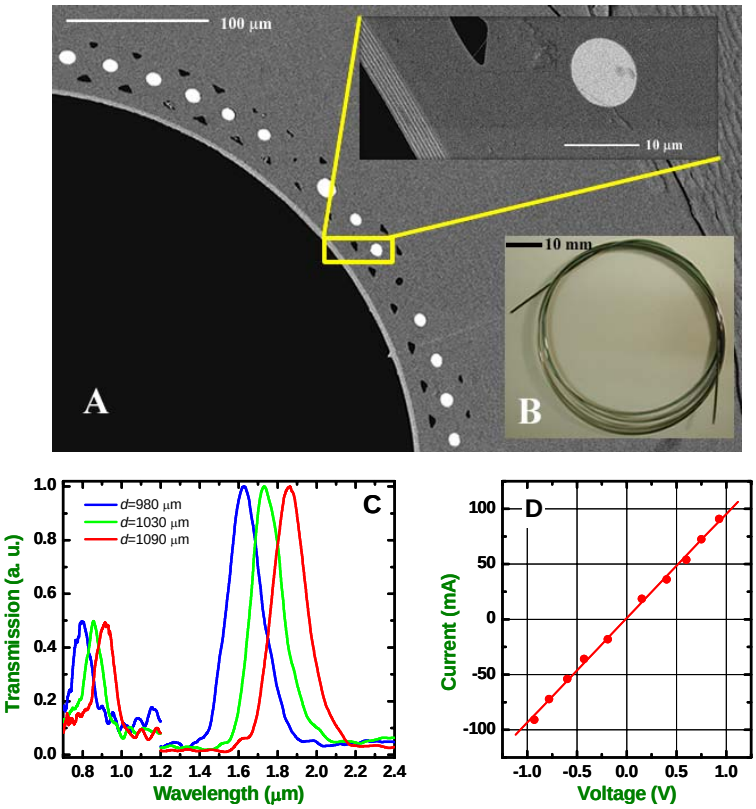

Figure 1 Dual electron-photon fibre (hybrid fibre). **A**, SEM micrograph of the cross section of the hybrid fibre with 800-μm hollow core, omnidirectional mirror layers, metallic filament array, and polymer cladding. The inset shows 8 pairs of quarter wave As_2Se_3/PEI multilayers and one of the metallic, Sn, filaments in the ring which is surrounding the mirror layers. **B,** Photograph of a 1-mm thick, 1-m long hybrid fibre. The fibre appears green to the eye by virtue of reflection from the third-order photonic band gap of the omnidirectional mirror, located at 550 nm. **C**, Normalized transmission spectra of three different fibres, having outer diameters of 980, 1030, and 1090 μm. The primary and second order photonic band gaps are located at 1.62 μm and 0.8 μm for the 980-μm thick fibre, and are shifted to longer wavelengths as the fibre diameter increases. **D,** Measured electrical current along the 980-μm thick fibre, 15 cm long, as a function of applied bias voltage.

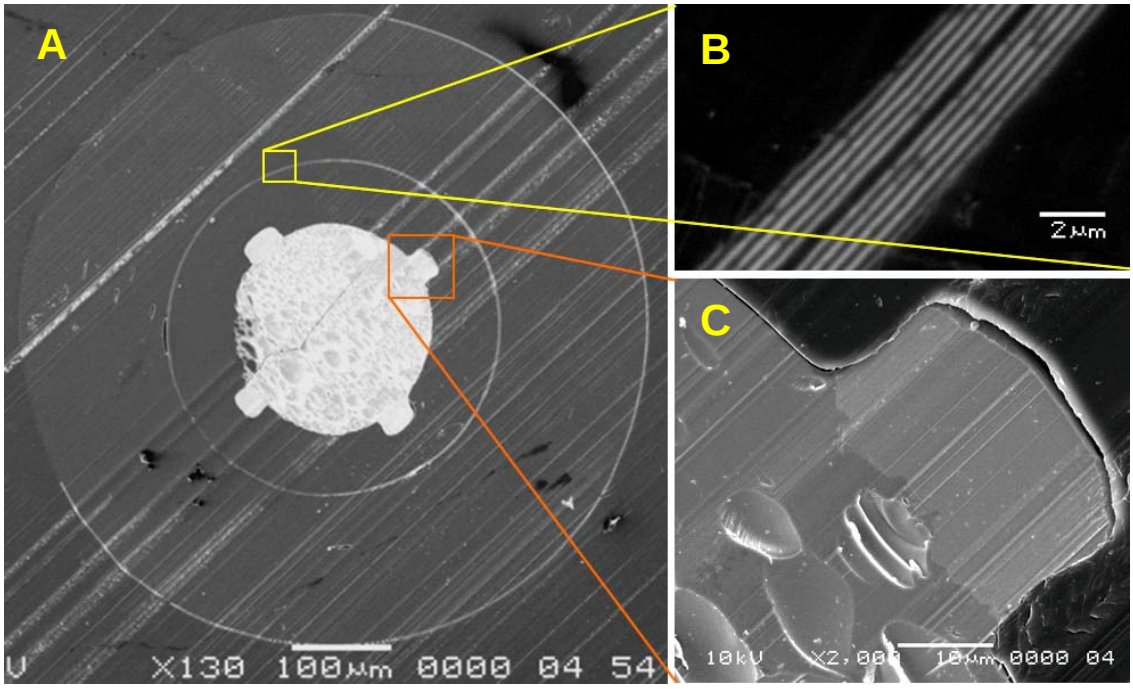

Figure 2 Integrated optoelectronic device fibre. **A**, SEM micrograph of the entire cross section of a 650-μm thick device fibre with 200-μm chalcogenide glass core surrounded by a PES cladding. The core region is surrounded by a resonant cavity structure (8 pairs of $\lambda/4$ As_2Se_3/PEI multilayers, with a $\lambda/2$ resonant cavity in the middle). The bright regions on the polymer-glass interface are the Sn metal electrodes, 18-μm thick and 30-μm wide, which are continuous along the whole fibre length. **B**, A magnified micrograph showing the resonant optical cavity structure. **C**, A magnified micrograph demonstrating the excellent quality of the semiconductor-metal interface.

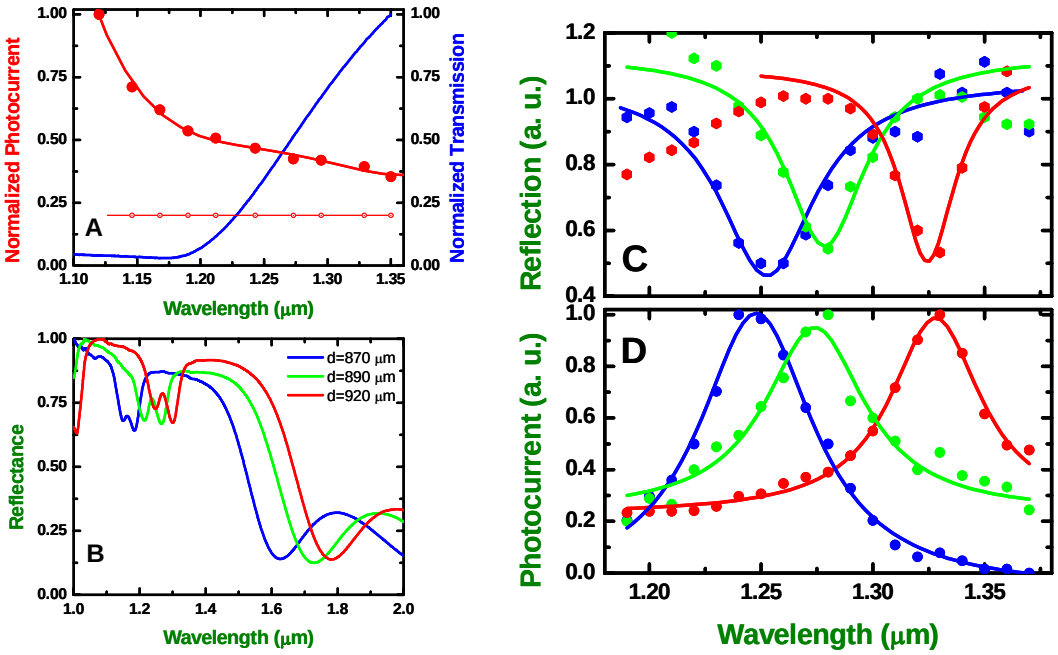

Figure 3 Results of optical and electrical measurements performed on the device fibres. **A**, The red curve is the normalized electrical current measured when illuminating a 890-μm two-electrode fibre, not equipped with a multilayer structure. The horizontal red line indicates the dark current level. The illumination was derived from a tunable OPO (Coherent), and the wavelength was swept while keeping the optical power constant. The blue curve shows the normalized transmission of a bulk AST-Sn glass sample. **B**, FTIR measured spectra of device fibres with 870, 900, and 910-μm outer diameter. **C**, Measured back-reflected light power from the same three device fibres when illuminated with a tunable OPO laser beam. **D**, Simultaneously measured photocurrent through the device fibre. Note that at the location of the resonance, the back-reflection is diminished (light is admitted into the fibre and reaches the photoconductive core) while the corresponding photocurrent, consequently, is enhanced.

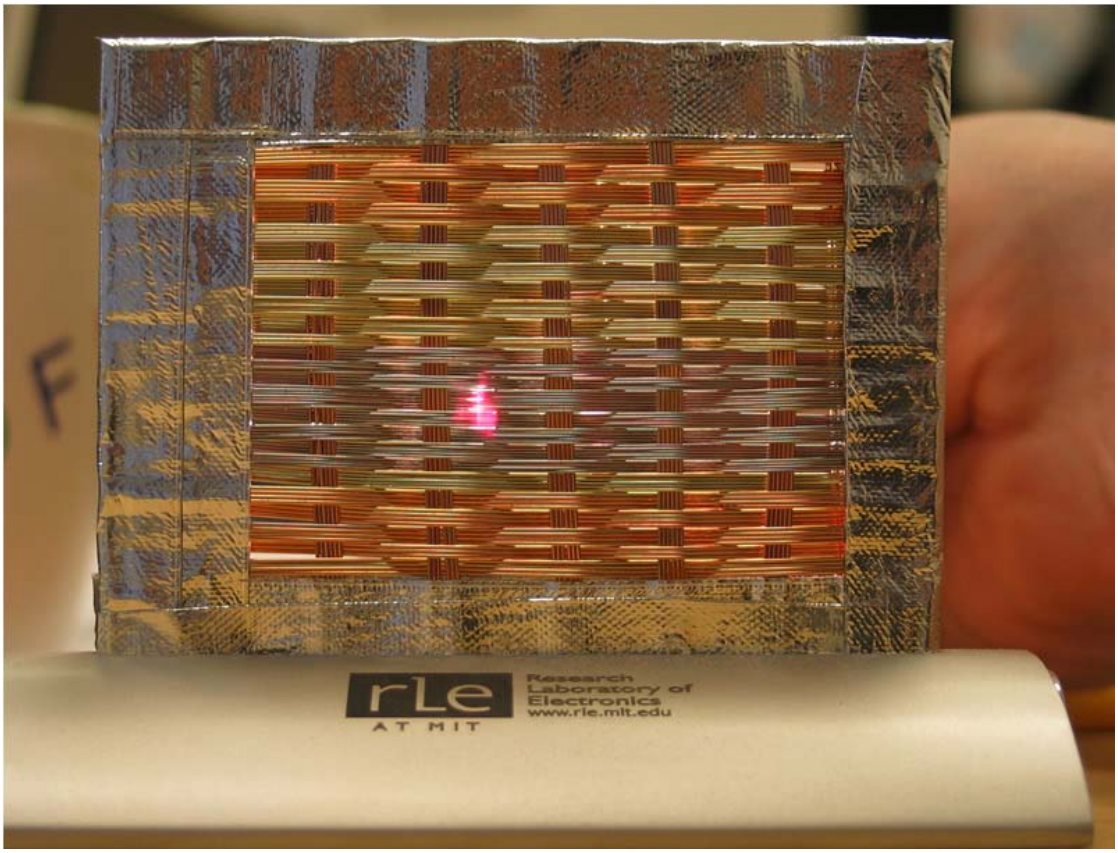

Figure 4 A woven spectrometric fabric. The fabric consists of interleaved threads, 400 to 500-μm thick, chosen from our device fibres. The visual appearance of the fabric, specifically the range of exhibited colors, is a result of the tight control exerted over the optical properties of the produced fibres.